Running title: Plant calmodulin-dependent NAD^+ kinase

Identification of the Arabidopsis calmodulin-dependent NAD^+ kinase that sustains the elicitor-induced oxidative burst

Elisa Dell'Aglio[a,b], Cécile Giustini[a], Alexandra Kraut[c], Yohann Couté[c], Alex Costa[d], Guillaume Decros[e], Yves Gibon[e,f], Christian Mazars[g], Michel Matringe[a], Giovanni Finazzi[a], Gilles Curien[a]*

[a] Univ. Grenoble Alpes, CNRS, CEA, INRA, BIG-LPCV, 38000 Grenoble, France

[b] Department of Botany and Plant Biology, University of Geneva, 1211 Geneva, Switzerland

[c] Univ. Grenoble Alpes, CEA, INSERM, BIG-EdyP, 38000 Grenoble, France

[d] Department of Biosciences, University of Milan, 20133 Milan, Italy

[e] UMR1332 BFP, INRA, Univ. Bordeaux, Villenave d'Ornon, France

[f] MetaboHUB, Bordeaux, Villenave d'Ornon, France

[g] Laboratoire de Recherche en Sciences Végétales, Université de Toulouse, CNRS, UPS, 24, Chemin de Borde-Rouge, Auzeville, BP 42617, 31326 Castanet-Tolosan, France.

* To whom correspondence may be addressed. E-mail: gilles.curien@cea.fr

One-sentence summary: A long-sought calmodulin and Ca^{2+}-dependent NAD kinase that is conserved in the plant lineage is the missing link between Ca^{2+} signalling, metabolism and the oxidative burst.

Author contributions

E.D., C.M., G.F. and G.C. designed the experiments and analyzed the data; E.D., C.G., M.M., A.K., Y.C., A.C. G.F., C.M., G.D., Y.G. and G.C. conducted the experiments. E.D., G.F., C.M. and G.C. wrote the article with contributions from all the authors. G.C. agrees to serve as the author responsible for contact and ensures communication.

Abstract

NADP(H) is an essential cofactor of multiple metabolic processes in all living organisms, and in plants, NADP(H) is required as the substrate of Ca^{2+}-dependent NADPH oxidases, which catalyze a reactive oxygen species burst in response to various stimuli. While $NADP^+$ production in plants has long been known to involve a calmodulin (CaM)/Ca^{2+}- dependent NAD^+ kinase, the nature of the

enzyme catalyzing this activity has remained enigmatic, as has its role in plant physiology. Here, we used proteomic, biochemical, molecular and *in vivo* analyses to identify an Arabidopsis (*Arabidopsis thaliana*) protein that catalyzes $NADP^+$ production exclusively in the presence of CaM/Ca^{2+}. This enzyme, which we named NAD kinase-CaM dependent (NADKc), has a CaM-binding peptide located in its N-terminal region and displays peculiar biochemical properties as well as different domain organization compared to known plant NAD^+ kinases. In response to a pathogen elicitor, activity of NADKc, which is associated with the mitochondrial periphery, contributes to an increase in the cellular $NADP^+$ concentration and to the amplification of the elicitor-induced oxidative burst. Based on a phylogenetic analysis and enzymatic assays, we propose the CaM/Ca^{2+}-dependent NAD^+ kinase activity found in photosynthetic organisms is carried out by NADKc-related proteins. Thus, NADKc represents the missing link between Ca^{2+} signalling, metabolism and the oxidative burst.

Keywords: NAD^+ kinase, Calmodulin, Calcium, $NADP^+$, zeta toxin, flagellin22, *Arabidopsis thaliana*.

Introduction

As sessile organisms, plants have evolved mechanisms to react quickly to stress conditions, such as changes in temperature, salinity or pathogen attacks. A common response to stress is a cytosolic calcium (Ca^{2+}) influx followed by an apoplastic burst of reactive oxygen species (ROS) (Grant et al., 2000). This ROS burst is generated by plasma membrane NADPH oxidases known as respiratory burst oxidase homologs (RBOHs, Torres and Dangl, 2005) and in turn regulates adaptation mechanisms such as gene expression, epigenetic changes and long-distance signal transduction (Liebthal and Dietz, 2017; Choi et al., 2017; Chapman et al., 2019). RBOH oxidase activity is dependent on Ca^{2+} binding to their EF-hand domains and is stimulated by phosphorylation by Ca^{2+}-dependent protein kinases (Dubiella et al., 2013) as well as CIPK/CBL complexes (Calcineurin B-Like Protein -CBL-Interacting Protein Kinase, Drerup *et al*., 2013).

A rapid increase in the NADP(H) pool size is observed in response to plant treatment with a pathogen elicitor (Harding et al., 1997; Pugin et al., 1997) and may be required to sustain the ROS burst by fuelling RBOH proteins. Since most (~70-90%) of plant NAD^+ kinase activity is dependent on binding calmodulin (CaM) in its Ca^{2+}-loaded conformation (Anderson and Cormier, 1978) it was proposed (Harding et al., 1997) that the protein responsible for this activity may also be stimulated by the elicitor-induced Ca^{2+} influx. $NADP^+$ produced by this enzyme may then be converted to NADPH (the substrate of RBOH proteins) by NADP-isocitrate dehydrogenase (Mhamdi et al., 2010) or by the reducing branch of the oxidative pentose phosphate pathway (Pugin et al., 1997; Scharte et al., 2009).

Several studies have described the CaM/Ca^{2+}-dependent NAD^+ kinase activity in plants using partially purified enzymatic preparations from plant tissues. These studies allowed finding this protein activity in a wide variety of plant species (Dieter and Marmé, 1984; Delumeau et al., 2000; Turner et al, 2004), and characterizing its kinetic parameters (Delumeau et al., 2000; Turner et al., 2004) as well as its preferences for specific CaM and CaM-like isoforms (Turner et al., 2004). However, the protein responsible for CaM/Ca^{2+}-dependent NAD^+ kinase activity has not been identified. In particular, among the three Arabidopsis (*Arabidopsis thaliana*) NAD^+ kinases identified to date, the plastidial NADK2 binds CaM *in vitro* in a Ca^{2+}-dependent way (Dell'Aglio et al., 2013a; Turner et al., 2004),

but its activity does not require CaM binding (Turner et al., 2004). Thus, this lack of knowledge of the identity of the plant CaM-dependent NAD^+ kinase has prevented a thorough characterization of its role in plant physiology, and in particular in the production of the stress-induced ROS burst.

Here, we report the characterization of an Arabidopsis CaM/Ca^{2+}-dependent NAD^+ kinase that displays all the properties of the elusive enzyme. We show this NAD^+ kinase, which we named NADKc (for NAD kinase-CaM dependent), is associated with the mitochondrial periphery and is involved in sustaining the ROS burst induced by the bacterial elicitor flagellin22.

Results and discussion

NADKc is a CaM/Ca^{2+}-dependent NAD^+ kinase

We obtained an Arabidopsis protein extract enriched in CaM/Ca^{2+}-dependent NAD^+ kinase activity by a four-step purification procedure described in the Supplemental Materials and Methods. The last step consisted in binding the protein on a CaM-charged matrix in the presence of Ca^{2+} and its subsequent release with an excess of the Ca^{2+} chelator EGTA, ethylene glycol-bis(β-aminoethyl ether)-*N*,*N*,*N*′,*N*′-tetraacetic acid (Fig. S1). We then used mass spectrometry-based proteomics to identify proteins enriched in the EGTA elution compared to the Ca^{2+}-containing washing steps (Supplemental Table S1). We reasoned putative CaM/Ca^{2+}-dependent NAD^+ kinases should display the following characteristics: *i)* have a molecular weight between 50 and 65 kDa, to respect the size range previously calculated by Delumeau et al., 2000; *ii)* be annotated as ATP-binding proteins (but not as a protein kinase), since plant CaM-activated NAD kinase uses ATP as a substrate (Anderson and Cormier, 1978); *iii)* contain a predicted CaM-binding site (following the guidelines of Rhoads and Friedberg, 1997) and *iv)* have no previously assigned enzymatic activity. Our analysis revealed only one protein – encoded by the At1g04280 gene – that fulfilled all these criteria.

To confirm its CaM/Ca^{2+}-dependent NAD^+ kinase activity, we expressed the full-length recombinant protein coded by At1g04280 in *Escherichia coli* with an N-terminal His-tag. We compared the NAD^+ kinase activity of two *E. coli* extracts: one obtained from an At1g04280-expressing strain and the second from a strain containing an empty vector. As shown in Fig. 1A, no NAD^+ kinase activity

(which in our test was detected as an increase of absorbance at 340 nm) was detected in the *E. coli* strain containing the empty vector, not even after the addition of an excess of Ca^{2+} and of Arabidopsis Calmodulin 1 (AtCaM1). In contrast, addition of the At1g04280-expressing *E. coli* extract to the same reaction mixture immediately revealed NAD^+ kinase activity.

Activity measurements with a partially purified At1g04280 enzyme confirmed the lack of NAD^+ kinase activity in the absence of AtCaM1/Ca^{2+} and its appearance, within seconds, upon addition of both AtCaM1 and Ca^{2+}. This NAD^+ kinase activity was suppressed by EGTA and restored by the addition of an excess of Ca^{2+}, showing the CaM/Ca^{2+}-dependent enzyme activation is an all-or-none, reversible process (Fig. 1B). In contrast, while CaM/Ca^{2+}-dependent NAD^+ kinases have also been described in invertebrates, animal NAD^+ kinase activity is only slightly increased by CaM/Ca^{2+} addition. For example, CaM induces a 3.5-fold increase of the NADK-2 activity of the sea urchin *Strongylocentrotus purpuratus* (Love et al., 2015).

Based on these results, we identified the At1g04280 gene product as the long-sought CaM/Ca^{2+}-dependent NAD^+ kinase enzyme previously found in several plant species (Anderson and Cormier, 1978, Delumeau et al., 1998, Turner et al., 2004) and named it Arabidopsis "NADKc" for "NAD kinase-CaM dependent".

AtNADKc peculiar features in primary sequence and enzyme activity

The primary sequence of NADKc (Fig. 1C) contains: *i)* an N-terminal region predicted to contain a transmembrane helix (amino acids: 1-45); *ii)* a domain of unknown function (amino acids 46-225) that includes a conserved putative CaM-binding site (CBS, Fig S2A); and *iii)* a C-terminal kinase domain (amino acids 226-340) similar to bacterial type II zeta-toxin domains (Khoo et al., 2007), which is predicted to contain a conserved P-loop for ATP binding (Walker A motif, WM, amino acids: 236-250, Fig S2B). Interestingly, these features are not shared with all other NAD^+ kinases known to date, from bacteria, plants and animals (Fig. 1C, Kawai et al, 2001; Turner et al., 2004, Chai et al., 2006; Love et al., 2015).

To optimize NADKc expression levels in *E. coli* and improve the solubility of the protein, we removed the first 38 residues constituting the predicted transmembrane helix. The shorter version, 6HIS-Δ38NADKc, was partially purified by Ni-NTA affinity chromatography (Fig. S3, lane 3). Activity assays with saturating AtCaM1/Ca^{2+} concentrations revealed the NAD^+ kinase activity of NADKc was specific toward NAD^+, as no activity could be detected with NADH or deamido-NAD^+ (NAAD) (Table 1). Like most P-loop-containing kinases (Das et al., 2013), the enzyme displayed broad specificity for the phosphoryl donor, as ATP, CTP, GTP and UTP could be used interchangeably and produced similar efficiencies (Table 1). The enzyme catalytic constant with CTP or ATP was close to 40 s^{-1} in the presence of Ca^{2+} and AtCaM1, *i.e.* about 10-fold higher than that reported for plant CaM/Ca^{2+}-independent NAD^+ kinases and other NAD^+ kinases from bacteria and animals (0.5-7 s^{-1}, (Kawai et al., 2001; Chai et al., 2006; Love et al., 2015; Turner et al., 2004)).

To characterize the interaction of NADKc with CaM, we further purified the recombinant enzyme by urea denaturation and rapid dilution (see Supplemental Material & Methods). The refolded protein (Fig S3, lanes 4-5) produced a single band on an SDS-PAGE gel and had an increased catalytic constant (70 s^{-1}) compared to the partially purified enzyme (40 s^{-1}, Table 1) and high affinity for CaM (k_d = 0.6-1 nM, Fig. 1D), similar to the value of 0.4 nM reported for the tomato (*Solanum lycopersicum*)CaM-dependent NAD^+ kinase (Delumeau et al., 2000).

In conclusion, compared to all other NAD^+ kinases known to date, NADKc displays unique structural as well as catalytic features which make it particularly suitable for rapid $NADP^+$ production following Ca^{2+} signals.

Identification of a CaM-binding peptide in the NADKc N-terminal domain

To verify the NADKc N-terminal domain is involved in CaM-binding, we measured NADKc activity in the presence of a synthetic peptide containing the putative “type A 1-8-14” CaM-binding sequence (amino acids 167-196, Fig. 1C, Rhoads and Friedberg, 1997) in a competitive assay. As shown in Fig. 1E, the presence of the putative NADKc CaM-binding peptide decreased the stimulation of NADKc by AtCaM1, as expected if AtCaM1, trapped by the peptide in excess, was no longer available for

NADKc activation. The reduction in reaction rate was hyperbolically related to the peptide concentration (IC50 =0.5 μM). In contrast, another unrelated peptide from the Short-chain dehydrogenase TIC 32 protein (At4g23430), which cannot specifically bind AtCaM1 (Dell'Aglio, 2013b), was also tested. An excess of this control peptide had no effect on NAD^+ kinase activity (Fig. 1E).

These data suggest the NADKc peptide identified plays a major role in the AtCaM1/Ca^{2+}-dependent activation of the NADKc enzyme. We hypothesize it could be an anchoring point for CaM in the full-length protein, facilitating activation of the kinase domain by an as yet unknown mechanism.

NADKc is located at the mitochondrial periphery

To assess the NADKc localization *in vivo*, we produced strains containing several YFP-tagged NADKc versions: *i.)* the NADKc full-length protein fused to YFP at its C-terminal (construct NADKc-YFP); *ii.)* the NADKc N-terminal region (amino acids 1-45) fused to YFP (construct $NADKc_{Nter}$-YFP); *iii)* the YFP fused at the N-terminus of the whole NADKc protein sequence (construct YFP-NADKc). All fusion proteins were inserted into expression plasmids under the control of the CaMV 35S promoter.

Arabidopsis lines and *Nicotiana benthamiana* leaves containing the NADKc:YFP construct showed protein clusters that likely constitute non-specific aggregates caused by high expression of a membrane construct (see Fig. S4 lower row). However, in *N. benthamiana* leaves (see Fig. S4, first and second row) and Arabidopsis seedlings, the $NADKc_{Nter}$-YFP was targeted to ring-like structures in both stomata (Fig. 2 A-F) and root tip cells (Fig. 2G-O). In the root tips, the $NADKc_{Nter}$-YFP protein co-localized with the mitochondrial matrix marker Tetramethylrhodamine, methyl ester (TMRM), but the fluorescence signal of $NADKc_{Nter}$-YFP was more peripheral than the TMRM signal (Fig. 2, G-I). As a comparison, we observed Arabidopsis root tip cells expressing NMT1-GFP, an outer mitochondrial membrane protein (Fig. 2, J-L, Wagner et al., 2015), as well as MT-cp-YFP (Fig. 2, M-O), a pH biosensor located in the mitochondrial matrix (Schwarzländer et al., 2011; Behera et al., 2018). This comparison clearly showed a higher resemblance of the $NADKc_{Nter}$-YFP signal profile to

the NMT1-GFP profile than to the MTcp-YFP profile, suggesting a localization at the outer mitochondrial membrane.

To corroborate this conclusion we measured the pixel intensity distribution of various TMRM-stained mitochondria from $NADKc_{Nter}$-YFP transformed plants. While the TMRM fluorescence intensity peak was located at the centre of the mitochondria, $NADKc_{Nter}$-YFP fluorescence intensity formed two distinctive peaks at opposite sides from the centre where fluorescence intensity was at its minimum (Fig. 2, P-R). This pattern matches the one previously measured for the outer-membrane localized NMT1-GFP protein (Wagner et al, 2015).

We successfully achieved expression of YFP-NADKc only in transiently transformed *N. benthamiana* leaves, where fluorescence was dispersed inside the cytosol (Fig. S4, third row). This result was probably due to the NADKc N-terminus being hidden in the middle of the sequence and is consistent with the hypothesis that the N-terminal region of NADKc is important for the protein to be correctly addressed to the mitochondria.

Protein overexpression by a strong promoter such as CaMV 35S is prone to promote protein aggregates and overexpression artefacts. However, using cell fractionation, early works on the CaM/Ca^{2+}-dependent NAD^+ kinase activity in plants located this enzyme at the mitochondrial periphery (either inner or outer mitochondrial membrane) in both maize (*Zea mays*) (Dieter and Marmé, 1984; Sauer and Robinson, 1985) and oat (*Avena sativa*) (Pou de Crescenzo et al., 2001). More recently, NADKc was detected in the mitochondria by two proteomic studies (Klodmann et al., 2011, Wagner et al., 2015) and at the plasma membrane by one study (Mitra et al., 2009). Our results therefore corroborate and extend previous findings obtained using different approaches.

NADKc enhances flg22 response in Arabidopsis seedlings

To investigate the physiological role of NADKc, we analysed the two Arabidopsis T-DNA insertion lines SALK_006202 and GABI-KAT 311H11, hereafter called *nadkc-1* and *nadkc-2* (Fig. 3A). NADKc transcripts were reduced by more than 95% in both lines (Fig. 3B).

To confirm the unique role of NADKc for CaM/Ca^{2+}-dependent $NADP^+$ production in Arabidopsis seedlings, NAD^+ kinase activity was measured in protein extracts from Col-0 and mutant seedlings, both in the presence of trifluoroperazine (TFP) - a CaM inhibitor - and AtCaM1/Ca^{2+} (Fig. 3C). In Col-0 plants, the activity measured in the presence of AtCaM1/Ca^{2+} was more than 10-fold higher than in the presence of TFP, while in *nadkc-1/2* mutants, no difference was observed between the two conditions. In both mutants, activity levels were similar to those measured in Col-0 plants in the presence of TFP, confirming the absence of NADKc activity in these mutants. Consistent with these results, two complemented lines obtained by stably transforming *nadkc-1* with full-length NADKc under the control of the CaMV 35S promoter (lines *nadkc-1*_NADKc-1 and *nadkc-1*_NADKc-2) - had NADKc activity levels similar to Col-0 (Fig. 4D).

Neither *nadkc* mutant showed any visible growth impairment when grown under short day or long day photoperiods (Fig. S5, A-B) and photosynthetic parameters (F_v/F_m, ETR and NPQ, (Maxwell and Johnson, 2000)) were the same in all genotypes (Fig. S5, C-E). This suggests NADKc is not involved in photosynthesis-driven growth.

As CaM-dependent NAD^+ kinase activity was previously associated with the generation of the oxidative burst triggered by plant response to elicitors (Grant et al., 2000; Harding et al., 1997), we expected to observe a decrease in a pathogen elicitor-induced extracellular ROS burst in *nadkc-1/2* mutants coupled with lower NADP pools with respect to Col-0 seedlings.

We therefore exposed 7-day-old Arabidopsis seedlings to the bacterial elicitor flg22, followed by measurements of $NAD(P)^+$ and NAD(P)H concentrations and ROS production. As shown in Fig. 3E, no statistically significant differences were observed between Col-0 and *nadkc-1* in $NAD(P)^+$ and NAD(P)H concentrations before the flg22 treatment. However, the flg22 challenge induced an increase in the Col-0 $NADP^+$ cellular concentration, which was absent in the *nadkc* seedlings. Moreover, dramatic reduction in ROS accumulation (more than 90%) was observed in the *nadkc-1/2* mutants (Fig. 3F), but complementation with the NADKc full-length protein restored ROS accumulation up to wild-type levels (Fig. 3G).

Based on these results, we propose a role for NADKc in producing NADP(H) needed to sustain the elicitor-induced ROS burst in Arabidopsis seedlings (Fig. 4).

Distribution of CaM-dependent NAD^+ kinase activity in the green lineage

The domain organization of NADKc (*i.e.*, a ca 200 amino acid domain of unknown function at the N-terminus with a putative CBS followed by a kinase domain annotated "zeta toxin domain", Fig. 1C) was only found in angiosperms, bryophytes and some algae.

To better trace the evolution of the plant CaM-dependent NAD^+ kinase, we compared gene sequences and NADK activity in several plants and algae, and we built a maximum likelihood phylogenetic tree with representative putative NADKc proteins (Fig. S6). The phylogenetic tree showed plant NADKc-like proteins form four major clusters that correspond to the main plant phylogenetic groups with the exception of gymnosperms and pteridophytes. Many plants, especially dicots, contain several genes encoding this protein, suggesting duplication events across evolution. Interestingly, the two other NADKc homologues present in the Arabidopsis genome (At1g06750 and At2g30630) seem to have a pollen-specific expression pattern (Krishnakumar et al., 2014).

Among algae, while the genomes of *Chlamydomonas reinhardtii*, *Ostreococcus taurii* and *Chara braunii* appeared devoid of NADKc-like sequences, the genomes of *Coccomyxa subellipsoidea*, *Ulva mutabilis*, *Klebsormidium flaccidum*, *Spyrotaenia minuta*, *Entransia fimbriata*, Mougeotia sp. and Spirogyra sp. all harbour one NADKc-like sequence. In particular, NAD^+ kinase genes of *K. flaccidum*, *E. fimbriata*, Mougeotia sp. and Spirogyra sp. contain a clear CBS, while in *C. subellipsoidea*, *U. mutabilis* and *S. minuta*, this region is less conserved (Fig. S2A). In agreement with the genomic survey, CaM-dependent NAD^+ kinase activity could be successfully measured in the moss *Marchantia polymorpha* and filamentous alga *K. flaccidum*, but not in the unicellular alga *C. reinhardtii* (Table 2).

Interestingly, both the total CaM-dependent NAD^+ kinase activity and the percentage of CaM-dependent NADK activity on the total NADK activity increase from *K. flaccidum* (4.0 $nmol \cdot h^{-1} \cdot mg^{-1}$; 66.7%) to *M. polymorpha* (5.9 $nmol \cdot h^{-1} \cdot mg^{-1}$; 85.7%) and to Arabidopsis (30.2 $nmol \cdot h^{-1} \cdot mg^{-1}$; 96.8%).

It is therefore possible the importance of the CaM control on NADKc-like proteins increased during the evolution of plant lineage and became a key element of the ROS response to elicitors in angiosperms, and quite likely other abiotic/biotic stress conditions that trigger Ca^{2+} fluxes.

Conclusions

Overall, we have identified unambiguously NADKc as the CaM/Ca^{2+}-dependent NAD^{+} kinase of Arabidopsis seedlings. Its identification allows answering earlier questions concerning its physiological role: consistent with its localization at the mitochondrial periphery, this enzyme has no role in photosynthesis but can regulate the ROS burst by sustaining the activity of RBOH proteins. Besides being essential for the elicitor-induced oxidative burst of Arabidopsis, this enzyme may participate in other plant developmental and stress responses involving Ca^{2+} fluxes. This would stem from the evolutionary recruitment of a distinctive combination of a CaM-binding region and a type II zeta-toxin domain, which would provide it with regulatory properties different from its animal counterpart.

Material and Methods

Chemicals

All chemicals were from Sigma Aldrich.

Plant growth and isolation of homozygous NADKc lines

Arabidopsis (*Arabidopsis thaliana*) Col-0 ecotype was used in this study. Plants were grown under 65% humidity and either long day (16 h light – 85 µmol photons·m^{-2}·s^{-1}, 8 h dark) or short day (8 h light – 90 µmol photons·m^{-2}·s^{-1}, 16 h dark) conditions. Day-time temperature was set to 20 °C, and night-time temperature to 18 °C.

The two T-DNA insertion lines, *nadkc-1* (SALK_006202) and *nadkc-2* (GABI_311H11), were obtained from NASC/ABRC (Alonso et al., 2003; Kleinboelting et al., 2012). Lines were selected in the appropriate antibiotic (kanamycin for *nadkc-1* and sulfadiazine for *nadkc-2*) and genotyped by

PCR using left border primers LBb1.3 (*nadkc-1*) or LB GABI-KAT (*nadkc-2*) and the appropriate specific primers listed in Supplemental Table S2. PCR products were sequenced to confirm the precise position of each insertion.

Klebsormidium flaccidum (Hori et al., 2014) (SAG335-2b curated as *Klebsormidium nitens*) was obtained from EPSAG (Department of Experimental Phycology and Culture Collection of Algae, Göttingen Universität, Germany). The alga was grown on agar plates under continuous light (60 µmol photons·m^{-2}·s^{-1}) in the Modified Bolds 3N Medium (https://utex.org/products/modified-bolds-3n medium) without vitamins.

Marchantia polymorpha was collected in the forest (GPS coordinate: 45.335088 , 5.632257) and *Chlamydomonas reinhardtii* (C137 strain) was grown in TAP medium at 24°C under continuous low white light (40 µmol photons·m^{-2}·s^{-1}) exposure. Protein extracts were prepared as described in the supplementary information for Arabidopsis.

Additional Material and Methods procedures are described in the Supplementary Information.

Accession numbers

Sequence data from this article can be found in the EMBL/GenBank data libraries under accession number: At1g04280; UniProt accession: Q0WUY1.

Supplemental Data

Figure legends

Supplemental Data

Supplemental Material and Methods

Supplemental Figure S1. CaM-affinity purification of native CaM-dependent NAD^+ kinase from Arabidopsis plantlets.

Supplemental Figure S2. Features of NADKc primary sequence and its homologues in other plant and algae species.

Supplemental Figure S3. Purification of recombinant NADKc produced in *E. coli*.

Supplemental Figure S4. A. $NADKc_{Nter}$-YFP associates with mitochondria in *N. benthamiana* leaves.

Supplemental Figure S5. Phenotype of *nadkc* mutants.

Supplemental Figure S6. Phylogeny of NADKc. Maximum likelihood phylogenetic tree of NADKc-like proteins in the following plant and algal species.

Supplemental Table S1. List of Arabidopsis proteins bound on CaM-affinity column in the presence of Ca^{2+} and eluted by EGTA identified by mass-spectrometry.

Supplementary Table S2. Primers used in this study.

Supplemental Figure S1. CaM-affinity purification of native CaM-dependent NAD^+ kinase from Arabidopsis plantlets. Proteins loaded and eluted from the CaM affinity chromatography column were separated by SDS-PAGE and stained with silver nitrate. In the "Loaded fraction", 24 µg in 38 µl were loaded; in the washings and EGTA elution fractions, 38 µl of each fraction were loaded (concentration not determined). Mass spectrometry-based proteomics was used to identify proteins strongly enriched in the EGTA elution compared to the Ca^{2+}-containing washing steps (Supplemental Table S1). Protein bands analysed by mass spectrometry are included in red boxes.

Supplemental Figure S2. Features of NADKc primary sequence and its homologues in other plant and algae species. (A) putative CaM binding site (Arabidopsis NADKc amino acids 167-200). Red residues are those constituting the 1-5-8-14 motif. This domain is not conserved in *C. subellipsoidea*, *U. mutabilis* and *S. minuta*. *A. thaliana*: *Arabidopsis thaliana*, *S. phallax*: *Sphagnum phallax*, *P. patens*: *Physcomitrella patens*, *M. polymorpha*: *Marchantia polymorpha*, *S. mollendorffii*: *Selaginella mollendorffii*, *S. lycopersicum*: *Solanum lycopersicum*, *G. max*: *Glycine max*, *M. truncatula*: *Medicago*

truncatula, *P. trichocarpa*: *Populus trichocarpa*, *M. acuminata*: *Musa acuminata*, *O. sativa*: *Oryza sativa*, *B. distachyon*: *Brachypodium distachyon*, *S. italica*: *Setaria italica*, *Z. mays*: *Zea mays*, *C. subellipsoidea*: *Coccomyxa subellipsoidea*, *U. mutabilis*: *Ulva mutabilis*, *S. minuta*: *Spirotaenia minuta*, *K. flaccidum*: *Klebsormidium flaccidum*, *E. fimbriata*: *Entransia fimbriata*. (B) Walker A motif (in red, residues characterizing the motif; *A. thaliana* NADKc amino acids 236-250). For gene references, see the legend of Fig. S6.

Supplemental Figure S3. Purification of recombinant NADKc produced in *E. coli*. 6HIS-Δ38NADKc was purified as indicated in Material and Methods. Lane 1: Rosetta2 soluble extract transformed with empty pET28a (40 µg); lane 2: Rosetta2 soluble extract transformed with pET28a6HIS-Δ38NADKc (40 µg); lane 3: Ni-NTA pool (10 µg); lane 4: urea-denatured 6HIS-Δ38NADKc purified on Ni-NTA (10 µg); lane 5: refolded 6HIS-Δ38NADKc (2 µg).

Supplemental Figure S4. A. NADKc$_{Nter}$-YFP associates with mitochondria in *N. benthamiana* leaves. Representative pictures of transiently transformed *N. benthamiana* leaf cells. Left: YFP (green), Center: RFP (red), and Right: merged fluorescence. The top row shows a representative image of *N. benthamiana* cells co-transformed with the NADKc$_{Nter}$-YFP construct and a mitochondrial marker, pSu9– RFP. The middle row shows a close-up of mitochondria from the lower right region of the images in the top row (white boxes). White arrows indicate regions in which the YFP signal appears peripheral with respect to the RFP signal. The bottom row shows a representative image of *N. benthamiana* cells transformed with the YFP-NADKc construct alone. The central image shows the background signal in the RFP channel. White bars represent 2 µm in the upper and second row, and 10 µm in the third row. **B**. Full length NADKc-YFP stably expressed in Arabidopsis forms aggregates in the cytosol. White bars represent 5 µm.

Supplemental Figure S5. Phenotype of *nadkc* mutants. (A) 21-day-old plants grown under long day photoperiod (16 h light/8 h dark); (B) 28-day-old plants grown under short day photoperiod (8 h light/16 h dark). (C-E) Photosynthetic parameters in Col-0 and *nadkc* plants: (C) NPQ, (D) Fv/Fm and (E) electron transport rate.

Supplemental Figure S6. Phylogeny of NADKc. Maximum likelihood phylogenetic tree of NADKc-like proteins in the following plant and algal species: *Arabidopsis thaliana* (*A. thaliana*), *Populus trichocarpa* (*P. trichocarpa*), *Manihot esculenta* (*M. esculenta*), *Gossypium raimondii* (*G. raimondii*), *Solanum lycopersicum* (*S. lycopersicum*), *Setaria italica* (*S. italica*), *Zea mays* (*Z. mays*), *Oryza sativa* (*O. sativa*), *Brachypodium distachyon* (*B. distachyon*), *Musa acuminata* (*M. acuminata*), *Marchantia polymorpha* (*M. polymorpha*), *Physcomitrella patens* (*P. patens*), *Sphagnum phallax* (*S. phallax*), *Selaginella mollendorffii* (*S. mollendorffii*) *Klebsormidium flaccidum* (*K. flaccidium*), *Coccomyxa subellipsoidea* (*C. subellipsoidea*), *Ulva mutabilis* (*U. mutabilis*), *Spirotaenia minuta* (*S. minuta*), Mougeotia sp., Spirogyra sp. and *Entransia fimbriata* (*E. fimbriata*). Accession numbers: *A. thaliana-1* (NADKc): At1g04280, *A. thaliana-2*: At1g06750, *A. thaliana-3*: At2g30630, *P. trichocarpa-1*: Potri.008G162000, *P. trichocarpa-2*: Potri.002G043000, *P. trichocarpa-3*: Potri.005G220000, *P. trichocarpa-4*: Potri.008G162400, *M. esculenta-1*: Manes.15G036900, *M. esculenta-2*: Manes.03G168900, *M. esculenta-3*: Manes.01G200600, *M. esculenta-4*: Manes.05G086200, *G. raimondii-1*: Gorai.011G171100, *G. raimondii-2*: Gorai.006G246600, *G. raimondii-3*: Gorai.004G074100, *G. raimondii-4*: Gorai.013G104300, *S. lycopersicum-1*: Solyc06g053810, *S. lycopersicum-2*: Solyc06g031670, *S. lycopersicum-3*: Solyc08g059750, *S. italica-1*: Seita.9G163700, *S. italica-2*: Seita.3G185100, *S. italica-3*: Seita.5G337000, *Z. mays-1*: GRMZM2G070252, *Z. mays-2*: GRMZM2G368410, *O. sativa-1*: Os03g43010, *O. sativa-2*: Os05g43300, *O. sativa-3*: Os01g56764, *B. distachyon-1*: Bradi1g14307, *B. distachyon-2*: Bradi2g51490, *B. distachyon-3*: Bradi2g20400, *M. acuminata-1*: SMUA_Achr5T03210, *M. acuminata-2*: GSMUA_Achr7T01560, *M. polymorpha*: Mapoly0142s0012, *P. patens*: Pp3c2_3490V3, *S. phallax-1*: Sphallax0059s0037, *S. phallax-2*: Sphallax0011s0002, *S. phallax-3*: Sphallax0120s0019, *S. mollendorffii-1*: scaffold 73427, *S. mollendorfii-2*: scaffold 231175, *K. flaccidum*: kfl00274_0130, *C. subellipsoidea*: XP_005648203, *U. mutabilis*: UM028_0076.1, *S. minuta*: NNHQ_2000691, *Mougeotia*: ZRMT_2002068, *Spirogyra*: HAOX_2025158, *E. fimbriata*: BFIK_2025349. The tree is drawn to scale, with branch lengths measured in the number of substitutions per site (scale bar in the bottom-left corner). The numbers at the interior nodes are bootstrap percentages.

Supplemental Table S1. List of Arabidopsis proteins bound on CaM-affinity column in the presence of Ca^{2+} and eluted by EGTA identified by mass-spectrometry.

Supplementary Table S2. Primers used in this study.

Acknowledgments

This work was supported by the French National Research Agency (grant no. ANR-10-13 LABEX-04 GRAL Labex, Grenoble Alliance for Integrated Structural Cell Biology). G.F. acknowledges support from the HFSP grant RGP0052/2015 (photosynthetic light utilization and ion fluxes: making the link) and A.C. to UNIMI PIANO DI SVILUPPO DI ATENEO, Transition Grant 2015/2017 – Horizon 2020 Linea 1A. The proteomic analyses were partially supported by the French National Research Agency ProFI Grant (ANR-16 10-INBS-08-01). Part of this work was carried out at NOLIMITS, an advanced imaging facility established by the University of Milan.

We are grateful to Markus Schwarzländer (University of Münster, Germany) for providing the NMT1:GFP and MT-cp:YFP Arabidopsis lines. We thank Elsa Clavel-Coibrié for help with analysis of the complemented mutant plants.

Tables

Table 1: NADKc kinetic parameters

Substrate varied	Constant substrate	K_M (µM)	k_{cat} (s^{-1})	k_{cat}/K_M ($\mu M^{-1}.s^{-1}$)
ATP	NAD^+ (10 mM)	203(±30)	41(±2)	0.2
CTP	NAD^+ (10 mM)	283(±70)	42(±1)	0.15
GTP	NAD^+ (10 mM)	522(±135)	26(±1)	0.05
UTP	NAD^+ (10 mM)	207(±26)	29.5(±2)	0.14
NAD^+	ATP (8 mM)	147 (±17)	42(±2)	0.28
$NADH^+$	ATP (8 mM)	n.d.	n.d.	n.d.

$NAAD^+$	ATP (8 mM)	n.d.	n.d.	n.d.

n.d.: not detected

Table 2: Comparison of CaM-dependent NADK activity in different photosynthetic organisms. NADK activity ($nmol \cdot h^{-1} \cdot mg^{-1}$ protein) was measured in soluble protein extracts from *Arabidopsis thaliana*, *Marchantia polymorpha*, *Klebsormidium flaccidum* and *Chlamydomonas reinhardtii* as detailed in the Materials and Methods. Activities are expressed in nmol/h/mg protein. [a]NADK activity measured in the presence of CaM/Ca^{2+} represents CaM-independent plus CaM–dependent activity; [b]NADK activity measured in the presence of trifluoroperazine (CaM inhibitor) represents CaM-independent NADK activity. [c]CaM/Ca^{2+}-dependent activity is the difference between total NADK activity and CaM/Ca^{2+}-independent activity. NADK activity in C. *reinhardtii* is independent of CaM/Ca^{2+} (the difference is within experimental error).

	A. thaliana	***M. polymorpha***	***K. flaccidum***	***C. reinhardtii***
Total activity[a]	31.2(±2.8)	6.9(±0.7)	5.8(±0.3)	24.6(±1.4)
CaM/Ca^{2+}-independent activity[b]	1.0(±0.3)	1.0(±0.1)	1.8(±0.3)	29.7(±2.7)
CaM/Ca^{2+}-dependent activity[c]	30.2	5.9	4.0	n.d.

n.d.: not detected.

Figures Legends

Figure 1. Biochemical properties of a CaM-dependent NAD^+ kinase identified in Arabidopsis. (A) NAD^+ kinase activity measured in an *E. coli* extract expressing an empty pET28b(+) and an *E. coli* extract expressing At1g04280. Spikes correspond to the moments of addition of glucose 6-phosphate dehydrogenase (G6PDH), Ca^{2+}, AtCaM1, and *E. coli* extracts (10 μg). (B) NAD^+ kinase activity in an *E. coli* bacterial extract expressing At1g04280. Ca^{2+}, AtCaM1 and EGTA were added at different

times, as indicated in the graph. (C) Schematic representation of the NADKc primary sequence and comparison with previously known NAD^+ kinases. Yellow: zeta-toxin domain (InterPro Homologous superfamily: IPR010488); black: N-terminal region with putative organelle target sequence; red: putative conserved Type A 1-8-14 CaM-binding site (detailed below the scheme); orange: Walker A motif (ATP-binding site); blue: NAD^+ kinase domain (InterPro Homologous Superfamily: IPR016064); red/grey: N-terminal sequence expected to contain a CaM-binding site according to Love et al, 2015. Sequences used for comparison (UniProt): *E. coli* NAD^+ kinase: P0A7B3; Arabidopsis NAD^+ kinases: AtNADK1: Q56YN3; AtNADK2: Q9C5W3; AtNADK3: Q500Y9; *Strongylocentrotus purpuratus* NAD^+ kinase-2 (sea urchin CaM-dependent NAD^+ kinase, Love et al., 2015): C3RSF7. (D) Affinity of NADKc recombinant protein for AtCaM1: Activity of the purified NADKc recombinant protein after denaturation in urea and subsequent refolding was measured in the presence of 50 µM Ca^{2+} and as a function of [AtCaM1]. Experiments were performed in triplicate and data shown are from one representative experiment. Binding data were analysed assuming tight binding. K_d value for AtCaM1 binding varied from 0.6 to 1 nM. (E) Inhibition of NADKc activity by competition with the putative CaM-binding site (black dots). Black squares correspond to results obtained with a negative control peptide, which does not bind AtCaM1.

Figure 2. Analysis of submitochondrial localization of $NADKc_{Nter}$-YFP. (A to C) Confocal laser scanning microscopy images from stomata guard cells of a representative Arabidopsis seedling stably expressing $NADKc_{Nter}$-YFP. Scale bar = 5 µm. (D to E) Higher magnification of the region of interest shown in A to C (white squares). Scale bar = 1 µm. (A, D) YFP fluorescence in green; (B, E) chlorophyll fluorescence in blue; (C, F) merged YFP and chlorophyll fluorescences. (G to I) Confocal laser scanning microscopy images from root tip cells of a representative Arabidopsis seedling stably expressing $NADKc_{Nter}$-YFP and stained with the mitochondrial matrix marker TMRM. Scale bar = 1 µm. (J to L) Confocal laser scanning microscopy images from root tip cells of a representative Arabidopsis seedling stably expressing NMT-GFP and stained with the mitochondrial matrix marker TMRM. Scale bar = 1 µm. (M to O) Confocal laser scanning microscopy images from root tip cells of a representative Arabidopsis seedling stably expressing MT-cpYFP and stained with the mitochondrial matrix marker TMRM. Scale bar = 1 µm. (G, M) YFP fluorescence in green; (J) GFP fluorescence in

green; (H, K and N) TMRM fluorescence in magenta; (I, L and O) merged YFP/GFP and TMRM fluorescences. NMT1-GFP and MT-cpYFP were used as markers for the outer mitochondrial membrane (OMM) and matrix, respectively. (P to R) Normalized pixel intensity distributions in the YFP and TMRM fluorescence channels plotted centrally across three individual mitochondria of a seedling expressing the $NADKc_{Nter}$-YFP.

Figure 3. The CaM/Ca^{2+}-dependent NAD^+ kinase activity of Arabidopsis seedlings is absent in *nadkc* mutants. (A) Schematic representation of the *NADKc* gene and position of the T-DNA insertions in the *nadkc-1* and *nadkc-2* mutant lines. (B) *NADKc* transcript levels in Col-0 and *nadkc*-mutant seedlings. Levels are expressed relative to those of *GAPDH*. Data shown correspond to mean +/- s.d., n=3. (C) NAD^+ kinase activity measured in Col-0 and *nadkc* mutant plants (7-day-old whole plantlets) in the presence of the CaM inhibitor TFP (40 μM) or AtCaM1 (250 nM) and Ca^{2+} (0.5 mM). Data shown correspond to mean +/- s.d., n=4. (D) NAD^+ kinase activity measured in seven-day-old Col-0 and mutant whole plantlets complemented with *NADKc* (*nadkc-1*_NADKc-1 and *nadkc-1*_NADKc-2) in the presence of the CaM inhibitor TFP (40 μM) or of AtCaM1 (250 nM) and Ca^{2+} (0.5 mM). (E) $NAD(P)^+$ and NAD(P)H concentrations in 7-day-old seedlings exposed (flg22, 1 μM) or unexposed (H_2O) for 12 min. to the bacterial elicitor flagellin22. (80-100 mg of tissue per measurement; data shown correspond to mean +/- s.e.m. for 3 biological replicates). (F) Flg22 (1 μM)-induced oxidative burst in 7-day-old Col-0 and *nadkc* mutant seedlings (30 plantlets per well; data shown correspond to mean +/- s.d. for 4 wells). (G) Flg22 (1 μM)-induced oxidative burst in Col-0, *nadkc-1* mutant and mutant plants complemented with *NADKc* (*nadkc-1*_NADKc-1 and *nadkc-1*_NADKc-2); 7-day-old seedlings, 30 plantlets per well. Data shown correspond to mean +/- s.d. for 4 wells. Asterisks indicate a significant difference between two conditions based on a Welch's *t*-test (*$p < 0.05$; ***$p < 0.001$).

Figure 4. Hypothetical model of the role of CaM/Ca^{2+}-dependent NADKc in sustaining the flg22-induced oxidative burst in Arabidopsis seedlings. Numbers refer to known sequential events; red numbers highlight events related to NADKc activation: 1. binding of flg22 elicitor to the Fls2 receptor (Sun et al., 2013); 2. activation of proton efflux and Ca^{2+} influx; 3a. Ca^{2+}-dependent activation of CDPKs and CIPK/CBLs that phosphorylate RBOH proteins; 3b. Ca^{2+} binding to RBOH proteins; 3c. Ca^{2+} binding to CaM, leading to CaM structural modification and formation of the CaM/NADKc

complex; 4. activation of $NADP^+$ production by NADKc; 5. increased flux in the oxidative pentose phosphate pathway (OPPP), leading to a higher availability of NADPH; 6. production of the extracellular oxidative burst by NADPH oxidases (RBOH proteins).

Literature Cited

Alonso JM, Stepanova AN, Leisse TJ, Kim CJ, Chen H, Shinn P, Stevenson DK, Zimmerman J, Barajas P, Cheuk R, et al (2003) Genome-wide insertional mutagenesis of *Arabidopsis thaliana*. Science **301:** 653-657

Anderson JM, Cormier MJ (1978) Calcium-dependent regulation of NAD kinase. Biochem Biophys Res Commun **84:** 595-602

Behera S, Zhaolong X, Luoni L, Bonza MC, Doccula FG, De Michelis MI, Morris RJ, Schwarzländer M, Costa A (2018) Cellular Ca^{2+} signals generate defined pH signatures in plants. Plant Cell **30:** 2704-2719

Chai MF, Wei PC, Chen QJ, An R, Chen J, Yang S, Wang XC (2006) NADK3, a novel cytoplasmic source of NADPH, is required under conditions of oxidative stress and modulates abscisic acid responses in Arabidopsis. Plant J **47:** 665-674

Chapman JM, Muhlemann JK, Gayomba SR, Muday GK (2019) RBOH-Dependent ROS Synthesis and ROS scavenging by plant specialized metabolites to modulate plant development and stress responses. Chem Res Toxicol. **32:** 370-396

Choi WG, Miller G, Wallace I, Harper J, Mittler R, Gilroy S (2017) Orchestrating rapid long-distance signaling in plants with Ca^{2+}, ROS and electrical signals. Plant J **90:** 698-707

Dell'Aglio E, Giustini C, Salvi D, Brugiere S, Delpierre F, Moyet L, Baudet M, Seigneurin-Berny D, Matringe M, Ferro M, et al (2013a) Complementary biochemical approaches applied to the identification of plastidial calmodulin-binding proteins. Mol Biosyst **9:** 1234-1248

Dell'Aglio E (2013b) The regulation of plastidial proteins by calmodulins: Université de Grenoble.

Delumeau O, Renard M, Montrichard F (2000b) Characterization and possible redox regulation of the purified calmodulin-dependent NAD^+ kinase from *Lycopersicon pimpinellifolium*. Plant Cell Environ **23:** 1267-1273

Dieter P, Marme D (1984) A Ca^{2+}, Calmodulin-dependent NAD kinase from corn is located in the outer mitochondrial membrane. J Biol Chem **259:** 184-189

Drerup MM, Schlücking K, Hashimoto K, Manishankar P, Steinhorst L, Kuchitsu K, Kudla J. (2013) The Calcineurin B-like calcium sensors CBL1 and CBL9 together with their interacting protein kinase CIPK26 regulate the Arabidopsis NADPH oxidase RBOHF. Mol Plant. **6:** 559-69

Dubiella U, Seybold H, Durian G, Komander E, Lassig R, Witte CP, Schulze WX, Romeis T (2013) Calcium-dependent protein kinase/NADPH oxidase activation circuit is required for rapid defense signal propagation. Proc Natl Acad Sci USA. **110:** 8744-9

Grant M, Brown I, Adams S, Knight M, Ainsli A, Mansfield J (2000) The RPM1 plant disease resistance gene facilitates a rapid and sustained increase in cytosolic calcium that is necessary for the oxidative burst and hypersensitive cell death. Plant J **23:** 441-450

Harding SA, Oh SH, Roberts DM (1997) Transgenic tobacco expressing a foreign calmodulin gene shows an enhanced production of active oxygen species. Embo J **16:** 1137-1144

Kawai S, Mori S, Mukai T, Hashimoto W, Murata K (2001) Molecular characterization of Escherichia coli NAD kinase. Eur J Biochem **268:** 4359-65

Khoo SK, Loll B, Chan WT, Shoeman RL, Ngoo L, Yeo CC, Meinhart A (2007) Molecular and structural characterization of the PezAT chromosomal toxin-antitoxin system of the human pathogen *Streptococcus pneumoniae*. J Biol Chem **282:** 19606-19618

Kleinboelting N, Huep G, Kloetgen A, Viehoever P, Weisshaar B (2012) GABI-Kat SimpleSearch: new features of the *Arabidopsis thaliana* T-DNA mutant database. Nucleic Acids Res **40:** D1211-1215

Klodmann J, Senkler M, Rode C, Braun H-P (2011) Defining the protein complex proteome of plant mitochondria. Plant Phys **157:** 587–598

Krishnakumar V, Hanlon MR, Contrino S, Ferlanti ES, Karamycheva S, Kim M, Rosen BD, Cheng C-Y, Moreira W, Mock SA, Stubbs J, Sullivan JM, Krampis K, Miller JR, Micklem G, Vaughn M, Town CD (2015) Araport: the Arabidopsis information portal. Nucleic Acids Research **43:** D1003–D1009

Love NR, Pollak N, Dolle C, Niere M, Chen Y, Oliveri P, Amaya E, Patel S, Ziegler M (2015) NAD kinase controls animal NADP biosynthesis and is modulated via evolutionarily divergent calmodulin-dependent mechanisms. Proc Natl Acad Sci USA **112:** 1386-1391

Liebthal M, Dietz KJ (2017) The fundamental role of reactive oxygen species in plant stress response. Plant Stress Tolerance In: Sunkar R. (eds) Plant Stress Tolerance. Methods in Molecular Biology, **1631:** 23-39. Humana Press, New York, NY.

Maxwell K, Johnson GN (2000) Chlorophyll fluorescence-a practical guide. J Exp Bot **51:** 659-668.

Mhamdi A, Mauve C, Gouia H, Saindrenan P, Hodges M, Noctor G (2010) Cytosolic NADP-dependent isocitrate dehydrogenase contributes to redox homeostasis and the regulation of pathogen responses in Arabidopsis leaves. Plant Cell Env **33:** 1112-1123

Mitra SK, Gantt JA, Ruby JF, Clouse SD, Goshe MB (2007) Membrane proteomic analysis of *Arabidopsis thaliana* using alternative solubilization techniques. J. Proteome Res. **6:** 1933-1950

Pou de Crescenzo M-A, Gallais S, Léon A, Laval-Martin DL (2001) Tween-20 activates and solubilizes the mitochondrial membrane-bound, calmodulin dependent NAD^+ kinase of *Avena sativa* L. J Membr Biol **182:** 135–146

Pugin A, Frachisse JM, Tavernier E, Bligny R, Gout E, Douce R, Guern J (1997) Early events induced by the elicitor cryptogein in tobacco cells: involvement of a plasma membrane NADPH oxidase and activation of glycolysis and the pentose phosphate pathway. Plant Cell **9:** 2077-2091

Rhoads AR, Friedberg F (1997) Sequence motifs for calmodulin recognition. The FASEB Journal **11:** 331–340

554 **Sauer A, Robinson DG** (1985) Calmodulin dependent NAD-kinase is associated with both the
555 outer and inner mitochondrial membranes in maize roots. Planta **166:** 227-233

556 **Scharte J, Schön H, Tjaden Z, Weis E, von Schaewen A** (2009) Isoenzyme replacement of
557 glucose-6-phosphate dehydrogenase in the cytosol improves stress tolerance in plants. Proc Natl Acad
558 Sci U S A **106:** 8061-8066

559 **Schwarzländer M, Logan DC, Fricker MD, Sweetlove LJ** (2011) The circularly permuted
560 yellow fluorescent protein cpYFP that has been used as a superoxide probe is highly responsive to pH
561 but not superoxide in mitochondria: implications for the existence of superoxide 'flashes'. Biochem J.
562 **437:** 381-7

563 **Torres MA, Dangl JL** (2005) Functions of the respiratory burst oxidase in biotic interactions,
564 abiotic stress and development. Curr Opin Plant Biol **8:** 397-403

565 **Turner WL, Waller JC, Vanderbeld B, Snedden WA** (2004). Cloning and characterization of
566 two NAD kinases from Arabidopsis. Identification of a calmodulin binding isoform. Plant Physiol
567 **135:** 1243-1255

568 **Wagner S, Behera S, De Bortoli S, Logan DC, Fuchs P, Carraretto L, Teardo E, Cendron**
569 **L, Nietzel T, Füßl M, Doccula FG, Navazio L, Fricker MD, Van Aken O, Finkemeier I, Meyer**
570 **AJ, Szabò I, Costa A, Schwarzländer M** (2015) The EF-hand Ca^{2+} binding protein MICU
571 choreographs mitochondrial Ca^{2+} dynamics in Arabidopsis. The Plant Cell **27:** 3190–3212

572

573

Figure 1

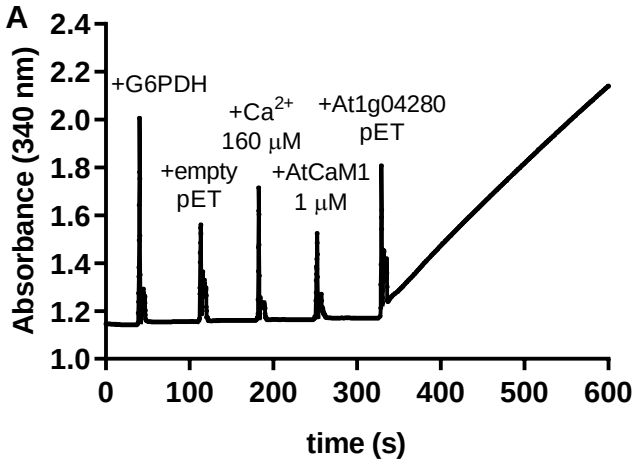

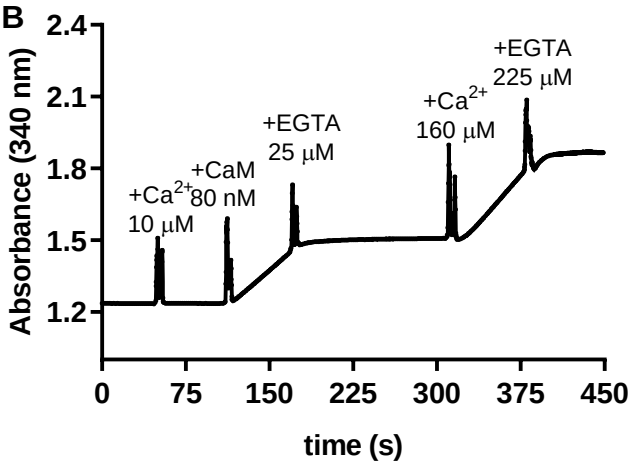

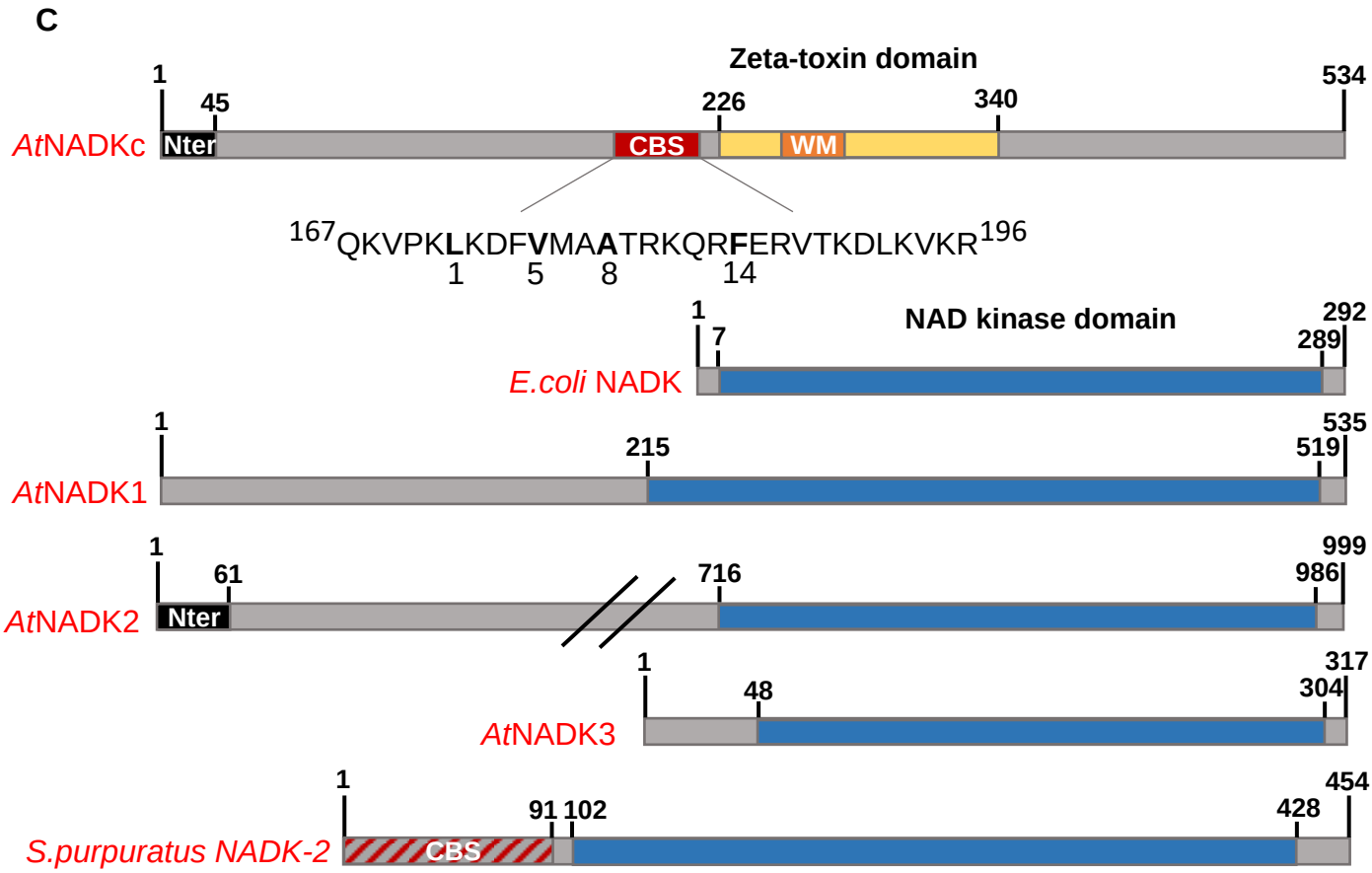

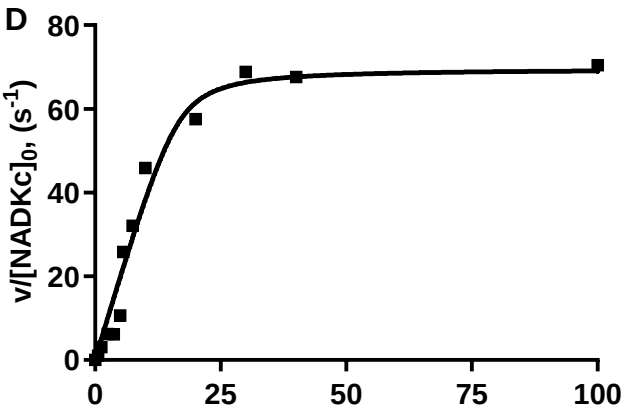

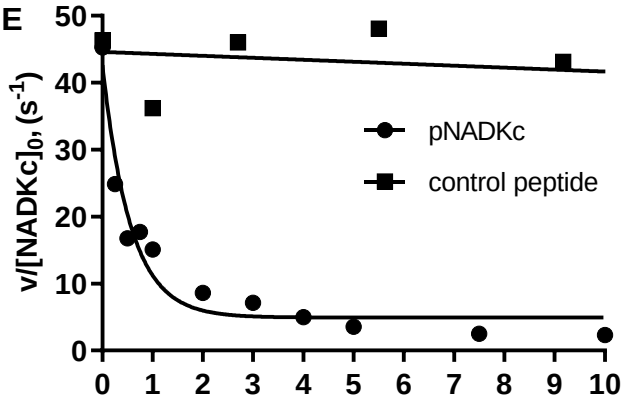

Figure 1. Biochemical properties of a CaM-dependent NAD^+ kinase identified in Arabidopsis. (A) NAD^+ kinase activity measured in an *E. coli* extract expressing an empty pET28b(+) and an *E. coli* extract expressing At1g04280. Spikes correspond to the moments of addition of glucose 6-phosphate dehydrogenase (G6PDH), Ca^{2+}, AtCaM1, and *E. coli* extracts (10 μg). (B) NAD^+ kinase activity in an *E. coli* bacterial extract expressing At1g04280. Ca^{2+}, AtCaM1 and EGTA were added at different times, as indicated in the graph. (C) Schematic representation of the NADKc primary sequence and comparison with previously known NAD^+ kinases. Yellow: zeta-toxin domain (InterPro Homologous superfamily: IPR010488); black: N-terminal region with putative organelle target sequence; red: putative conserved Type A 1-8-14 CaM-binding site (detailed below the scheme); orange: Walker A motif (ATP-binding site); blue: NAD^+ kinase domain (InterPro Homologous Superfamily: IPR016064); red/grey: N-terminal sequence expected to contain a CaM-binding site according to Love et al, 2015. Sequences used for comparison (UniProt): *E. coli* NAD^+ kinase: P0A7B3; *A. thaliana* NAD^+ kinases: AtNADK1: Q56YN3; AtNADK2: Q9C5W3; AtNADK3: Q500Y9; *Strongylocentrotus purpuratus* NAD^+ kinase-2 (sea urchin CaM-dependent NAD^+ kinase, Love et al., 2015): C3RSF7. (D) Affinity of NADKc recombinant protein for AtCaM1: Activity of the purified NADKc recombinant protein after denaturation in urea and subsequent refolding was measured in the presence of 50 μM Ca^{2+} and as a function of [AtCaM1]. Experiments were performed in triplicate and data shown are from one representative experiment. Binding data were analysed assuming tight binding. K_d value for AtCaM1 binding varied from 0.6 to 1 nM. (E) Inhibition of NADKc activity by competition with the putative CaM-binding site (black dots). Black squares correspond to results obtained with a negative control peptide, which does not bind AtCaM1.

Figure 2

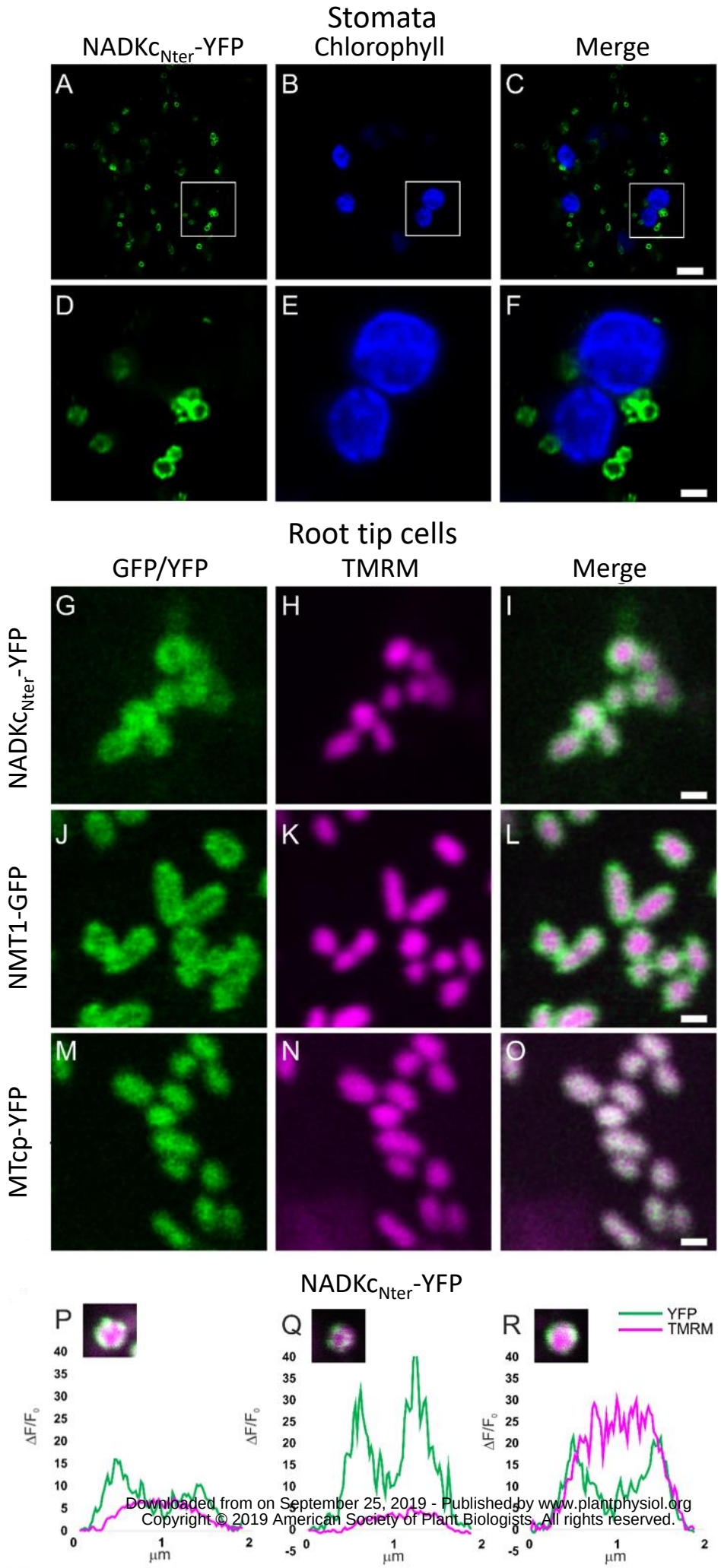

Figure 2. Analysis of submitochondrial localization of $NADKc_{Nter}$-YFP. (A to C) Confocal laser scanning microscopy images from stomata guard cells of a representative Arabidopsis seedling stably expressing $NADKc_{Nter}$-YFP. Scale bar = 5 µm. (D to E) Higher magnification of the region of interest shown in A to C (white squares). Scale bar = 1 µm. (A, D) YFP fluorescence in green; (B, E) chlorophyll fluorescence in blue; (C, F) merge between YFP and chlorophyll fluorescences. (G to I) Confocal laser scanning microscopy images from root tip cells of a representative Arabidopsis seedling stably expressing $NADKc_{Nter}$-YFP and stained with the mitochondrial matrix marker TMRM. Scale bar = 1 µm. (J to L) Confocal laser scanning microscopy images from root tip cells of a representative Arabidopsis seedling stably expressing NMT-GFP and stained with the mitochondrial matrix marker TMRM. Scale bar = 1 µm. (M to O) Confocal laser scanning microscopy images from root tip cells of a representative Arabidopsis seedling stably expressing MT-cpYFP and stained with the mitochondrial matrix marker TMRM. Scale bar = 1 µm. (G, M) YFP fluorescence in green; (J) GFP fluorescence in green; (H, K and N) TMRM fluorescence in magenta; (I, L and O) merge between YFP/GFP and TMRM fluorescences. NMT1-GFP and MT-cpYFP were used as markers for the mitochondrial outer mitochondrial membrane (OMM) and matrix, respectively. (P to R) Normalized pixel intensity distributions in the YFP and TMRM fluorescence channels plotted centrally across three individual mitochondria of a seedling expressing the $NADKc_{Nter}$-YFP.

Figure 3

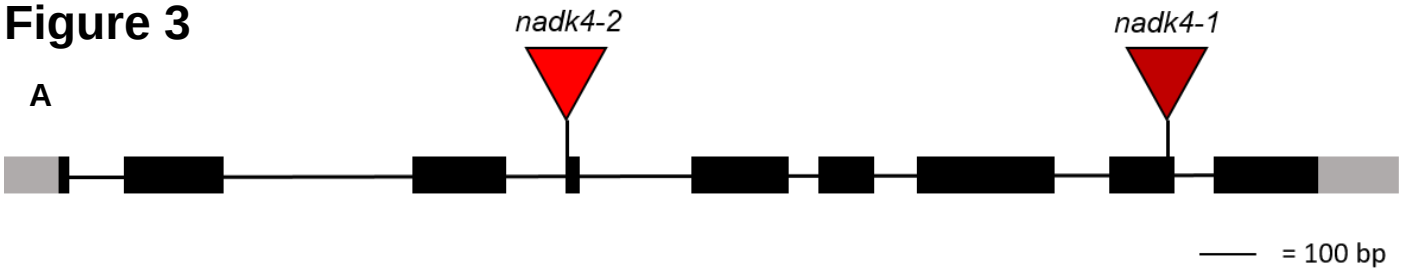

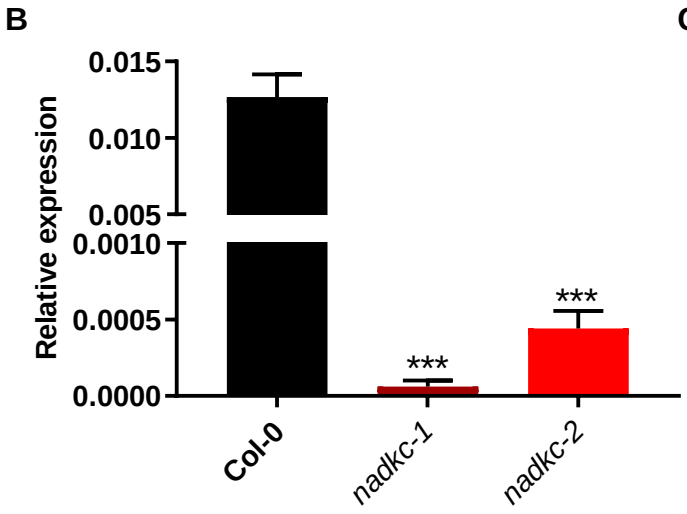

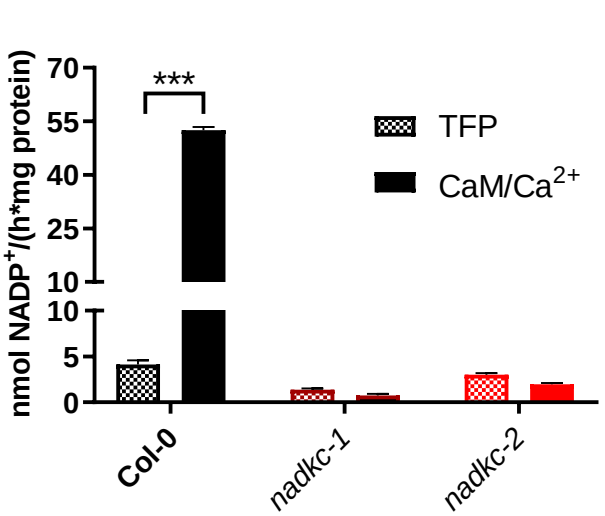

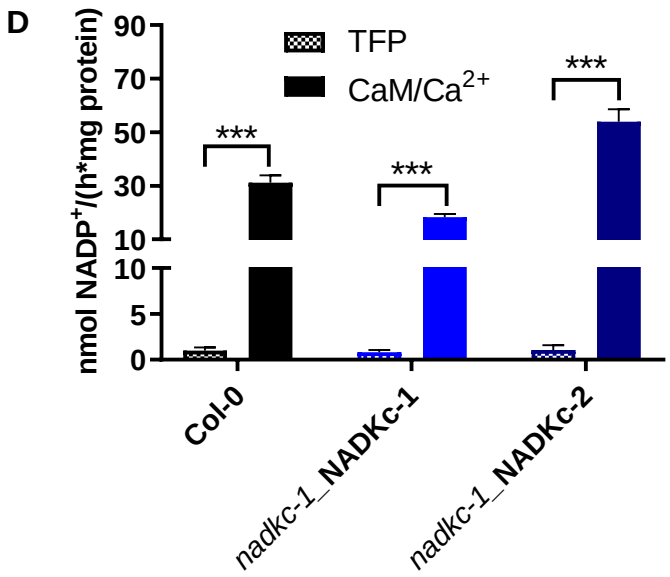

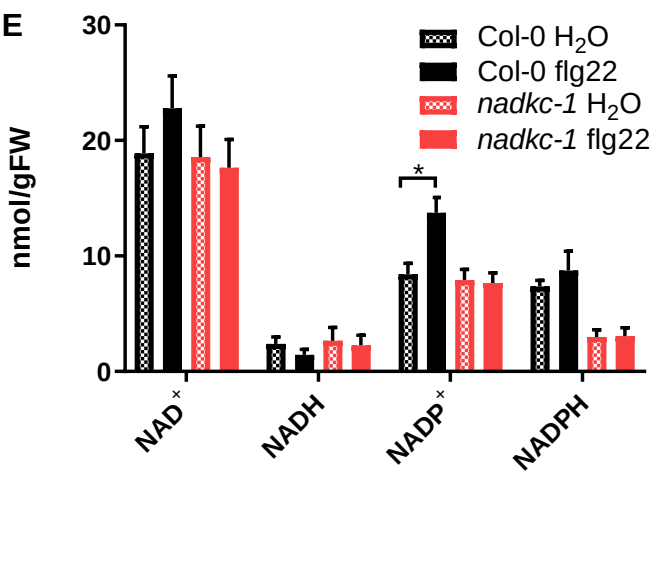

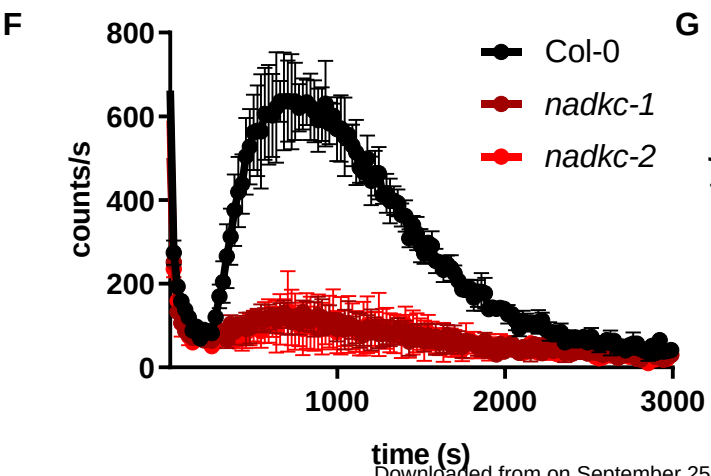

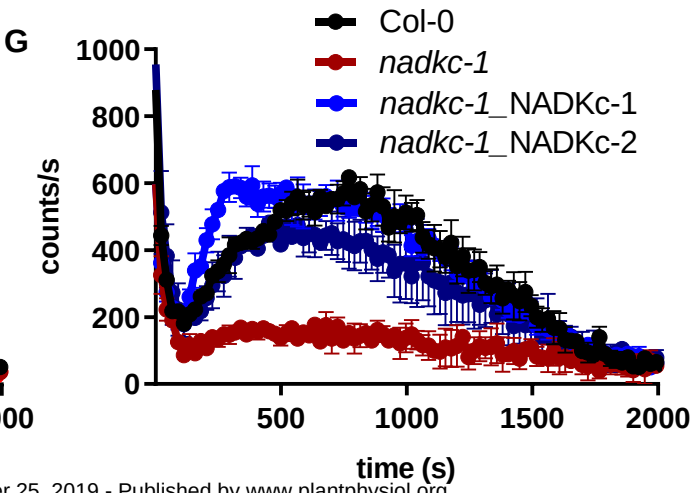

Figure 3. The CaM/Ca^{2+}-dependent NAD^+ kinase activity of Arabidopsis seedlings is absent in *nadkc* mutants. (A) schematic representation of the NADKc gene and position of the T-DNA insertions in the *nadkc-1* and *nadkc-2* mutant lines. (B) NADKc transcript levels in Col-0 and *nadkc*-mutant seedlings. Levels are expressed relative to GAPDH. Data shown correspond to mean +/- s.d., n=3. (C) NAD^+ kinase activity measured in Col-0 and *nadkc* mutant plants (7-day-old whole plantlets), in the presence of the CaM inhibitor TFP (40 μM) or AtCaM1 (250 nM) and Ca^{2+} (0.5 mM). Values correspond to the average of four replicates. (D) NAD^+ kinase activity measured in Col-0 and mutant plants complemented with NADKc gene (*nadkc-1*_NADKc-1 and *nadkc-1*_NADKc-2) in 7-day-old whole plantlets, in the presence of the CaM inhibitor TFP (40 μM) or of AtCaM1 (250 nM) and Ca^{2+} (0.5 mM). (E) $NAD(P)^+$ and NAD(P)H concentrations in 7-day-old seedlings exposed (flg22, 1 μM) or unexposed (H_2O) for 12 min. to the bacterial elicitor flagellin22. (80-100 mg of tissue per measure, data shown correspond to mean +/- s.e.m. for 3 biological replicates). (F) Flg22 (1 μM)-induced oxidative burst in 7-day-old Col-0 and *nadkc* mutant seedlings (30 plantlets per well, data shown correspond to mean +/- s.d. for 4 wells). (G) Flg22 (1 μM)-induced oxidative burst in Col-0, *nadkc-1* mutant and mutant plants complemented with NADKc gene (*nadkc-1*_NADKc-1 and *nadkc-1*_NADKc-2); 7-day-old seedlings, 30 plantlets per well. Data shown correspond to mean +/- s.d. for 4 wells. Asterisks indicate a significant difference between two conditions based on a Welch's t test (*$p < 0.05$; ***$p < 0.001$).

Figure 4

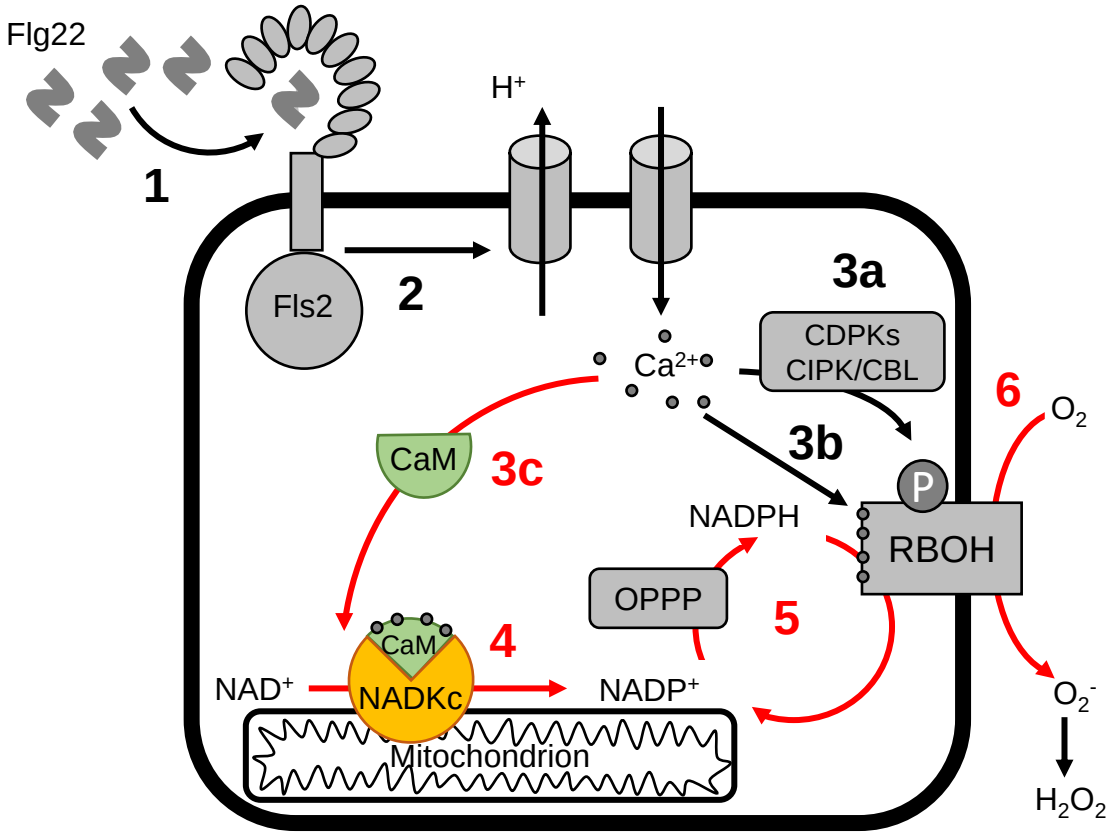

Figure 4. Hypothetical model of the role of CaM/Ca^{2+}-dependent NADKc in sustaining the flg22-induced oxidative burst in Arabidopsis seedlings. Numbers refer to known sequential events; red numbers highlight events related to NADKc activation: 1. binding of Flg22 elicitor to the Fls2 receptor (Sun et al., 2013); 2. activation of proton efflux and Ca^{2+} influx; 3a. Ca^{2+}-dependent activation of CDPKs and CIPK/CBLs that phosphorylate RBOH proteins; 3b. Ca^{2+} binding to RBOH proteins; 3c. Ca^{2+} binding to CaM, leading to CaM structural modification and formation of the CaM/NADKc complex; 4. activation of $NADP^{+}$ production by NADKc; 5. increased flux in the oxidative pentose phosphate pathway (OPPP), leading to a higher availability of NADPH; 6. production of the extracellular oxidative burst by NADPH oxidases (RBOH proteins).

Parsed Citations

Alonso JM, Stepanova AN, Leisse TJ, Kim CJ, Chen H, Shinn P, Stevenson DK, Zimmerman J, Barajas P, Cheuk R, et al (2003) Genome-wide insertional mutagenesis of Arabidopsis thaliana. Science 301: 653-657
Pubmed: Author and Title
Google Scholar: Author Only Title Only Author and Title

Anderson JM, Cormier MJ (1978) Calcium-dependent regulation of NAD kinase. Biochem Biophys Res Commun 84: 595-602
Pubmed: Author and Title
Google Scholar: Author Only Title Only Author and Title

Behera S, Zhaolong X, Luoni L, Bonza MC, Doccula FG, De Michelis MI, Morris RJ, Schwarzländer M, Costa A (2018) Cellular Ca2+ signals generate defined pH signatures in plants. Plant Cell 30: 2704-2719
Pubmed: Author and Title
Google Scholar: Author Only Title Only Author and Title

Chai MF, Wei PC, Chen QJ, An R, Chen J, Yang S, Wang XC (2006) NADK3, a novel cytoplasmic source of NADPH, is required under conditions of oxidative stress and modulates abscisic acid responses in Arabidopsis. Plant J 47: 665-674
Pubmed: Author and Title
Google Scholar: Author Only Title Only Author and Title

Chapman JM, Muhlemann JK, Gayomba SR, Muday GK (2019) RBOH-Dependent ROS Synthesis and ROS scavenging by plant specialized metabolites to modulate plant development and stress responses. Chem Res Toxicol. 32: 370-396
Pubmed: Author and Title
Google Scholar: Author Only Title Only Author and Title

Choi WG, Miller G, Wallace I, Harper J, Mittler R, Gilroy S (2017) Orchestrating rapid long-distance signaling in plants with Ca2+, ROS and electrical signals. Plant J 90: 698-707
Pubmed: Author and Title
Google Scholar: Author Only Title Only Author and Title

Dell'Aglio E, Giustini C, Salvi D, Brugiere S, Delpierre F, Moyet L, Baudet M, Seigneurin-Berny D, Matringe M, Ferro M, et al (2013a) Complementary biochemical approaches applied to the identification of plastidial calmodulin-binding proteins. Mol Biosyst 9: 1234-1248
Pubmed: Author and Title
Google Scholar: Author Only Title Only Author and Title

Dell'Aglio E (2013b) The regulation of plastidial proteins by calmodulins: Université de Grenoble.

Delumeau O, Renard M, Montrichard F (2000b) Characterization and possible redox regulation of the purified calmodulin-dependent NAD+ kinase from Lycopersicon pimpinellifolium. Plant Cell Environ 23: 1267-1273
Pubmed: Author and Title
Google Scholar: Author Only Title Only Author and Title

Dieter P, Marme D (1984) A Ca2+, Calmodulin-dependent NAD kinase from corn is located in the outer mitochondrial membrane. J Biol Chem 259: 184-189
Pubmed: Author and Title
Google Scholar: Author Only Title Only Author and Title

Drerup MM, Schlücking K, Hashimoto K, Manishankar P, Steinhorst L, Kuchitsu K, Kudla J. (2013) The Calcineurin B-like calcium sensors CBL1 and CBL9 together with their interacting protein kinase CIPK26 regulate the Arabidopsis NADPH oxidase RBOHF. Mol Plant. 6: 559-69
Pubmed: Author and Title
Google Scholar: Author Only Title Only Author and Title

Dubiella U, Seybold H, Durian G, Komander E, Lassig R, Witte CP, Schulze WX, Romeis T (2013) Calcium-dependent protein kinase/NADPH oxidase activation circuit is required for rapid defense signal propagation. Proc Natl Acad Sci USA. 110: 8744-9
Pubmed: Author and Title
Google Scholar: Author Only Title Only Author and Title

Grant M, Brown I, Adams S, Knight M, Ainsli A, Mansfield J (2000) The RPM1 plant disease resistance gene facilitates a rapid and sustained increase in cytosolic calcium that is necessary for the oxidative burst and hypersensitive cell death. Plant J 23: 441-450
Pubmed: Author and Title
Google Scholar: Author Only Title Only Author and Title

Harding SA, Oh SH, Roberts DM (1997) Transgenic tobacco expressing a foreign calmodulin gene shows an enhanced production of active oxygen species. Embo J 16: 1137-1144
Pubmed: Author and Title
Google Scholar: Author Only Title Only Author and Title

Kawai S, Mori S, Mukai T, Hashimoto W, Murata K (2001) Molecular characterization of Escherichia coli NAD kinase. Eur J Biochem 268: 4359-65
Pubmed: Author and Title
Google Scholar: Author Only Title Only Author and Title

Khoo SK, Loll B, Chan WT, Shoeman RL, Ngoo L, Yeo CC, Meinhart A (2007) Molecular and structural characterization of the PezAT chromosomal toxin-antitoxin system of the human pathogen Streptococcus pneumoniae. J Biol Chem 282: 19606-19618
Pubmed: Author and Title
Google Scholar: Author Only Title Only Author and Title

Kleinboelting N, Huep G, Kloetgen A, Viehoever P, Weisshaar B (2012) GABI-Kat SimpleSearch: new features of the Arabidopsis thaliana T-DNA mutant database. Nucleic Acids Res 40: D1211-1215
Pubmed: Author and Title
Google Scholar: Author Only Title Only Author and Title

Klodmann J, Senkler M, Rode C, Braun H-P (2011) Defining the protein complex proteome of plant mitochondria. Plant Phys 157: 587–598
Pubmed: Author and Title
Google Scholar: Author Only Title Only Author and Title

Krishnakumar V, Hanlon MR, Contrino S, Ferlanti ES, Karamycheva S, Kim M, Rosen BD, Cheng C-Y, Moreira W, Mock SA, Stubbs J, Sullivan JM, Krampis K, Miller JR, Micklem G, Vaughn M, Town CD (2015) Araport: the Arabidopsis information portal. Nucleic Acids Research 43: D1003–D1009
Pubmed: Author and Title
Google Scholar: Author Only Title Only Author and Title

Love NR, Pollak N, Dolle C, Niere M, Chen Y, Oliveri P, Amaya E, Patel S, Ziegler M (2015) NAD kinase controls animal NADP biosynthesis and is modulated via evolutionarily divergent calmodulin-dependent mechanisms. Proc Natl Acad Sci USA 112: 1386-1391
Pubmed: Author and Title
Google Scholar: Author Only Title Only Author and Title

Liebthal M, Dietz KJ (2017) The fundamental role of reactive oxygen species in plant stress response. Plant Stress Tolerance In: Sunkar R. (eds) Plant Stress Tolerance. Methods in Molecular Biology, 1631: 23-39. Humana Press, New York, NY.
Pubmed: Author and Title
Google Scholar: Author Only Title Only Author and Title

Maxwell K, Johnson GN (2000) Chlorophyll fluorescence-a practical guide. J Exp Bot 51: 659-668.
Pubmed: Author and Title
Google Scholar: Author Only Title Only Author and Title

Mhamdi A, Mauve C, Gouia H, Saindrenan P, Hodges M, Noctor G (2010) Cytosolic NADP-dependent isocitrate dehydrogenase contributes to redox homeostasis and the regulation of pathogen responses in Arabidopsis leaves. Plant Cell Env 33: 1112-1123
Pubmed: Author and Title
Google Scholar: Author Only Title Only Author and Title

Mitra SK, Gantt JA, Ruby JF, Clouse SD, Goshe MB (2007) Membrane proteomic analysis of Arabidopsis thaliana using alternative solubilization techniques. J. Proteome Res. 6: 1933-1950
Pubmed: Author and Title
Google Scholar: Author Only Title Only Author and Title

Pou de Crescenzo M-A, Gallais S, Léon A, Laval-Martin DL (2001) Tween-20 activates and solubilizes the mitochondrial membrane-bound, calmodulin dependent NAD+ kinase of Avena sativa L. J Membr Biol 182: 135–146
Pubmed: Author and Title
Google Scholar: Author Only Title Only Author and Title

Pugin A, Frachisse JM, Tavernier E, Bligny R, Gout E, Douce R, Guern J (1997) Early events induced by the elicitor cryptogein in tobacco cells: involvement of a plasma membrane NADPH oxidase and activation of glycolysis and the pentose phosphate pathway. Plant Cell 9: 2077-2091
Pubmed: Author and Title
Google Scholar: Author Only Title Only Author and Title

Rhoads AR, Friedberg F (1997) Sequence motifs for calmodulin recognition. The FASEB Journal 11: 331–340
Pubmed: Author and Title
Google Scholar: Author Only Title Only Author and Title

Sauer A, Robinson DG (1985) Calmodulin dependent NAD-kinase is associated with both the outer and inner mitochondrial membranes in maize roots. Planta 166: 227-233
Pubmed: Author and Title
Google Scholar: Author Only Title Only Author and Title

Scharte J, Schön H, Tjaden Z, Weis E, von Schaewen A (2009) Isoenzyme replacement of glucose-6-phosphate dehydrogenase in the cytosol improves stress tolerance in plants. Proc Natl Acad Sci U S A 106: 8061-8066
Pubmed: Author and Title
Google Scholar: Author Only Title Only Author and Title

Schwarzländer M, Logan DC, Fricker MD, Sweetlove LJ (2011) The circularly permuted yellow fluorescent protein cpYFP that has been used as a superoxide probe is highly responsive to pH but not superoxide in mitochondria: implications for the existence of superoxide 'flashes'. Biochem J. 437: 381-7
Pubmed: Author and Title
Google Scholar: Author Only Title Only Author and Title

Torres MA, Dangl JL (2005) Functions of the respiratory burst oxidase in biotic interactions, abiotic stress and development. Curr Opin Plant Biol 8: 397-403
Pubmed: Author and Title
Google Scholar: Author Only Title Only Author and Title

Turner WL, Waller JC, Vanderbeld B, Snedden WA (2004). Cloning and characterization of two NAD kinases from Arabidopsis. Identification of a calmodulin binding isoform. Plant Physiol 135: 1243-1255
Pubmed: Author and Title
Google Scholar: Author Only Title Only Author and Title

Wagner S, Behera S, De Bortoli S, Logan DC, Fuchs P, Carraretto L, Teardo E, Cendron L, Nietzel T, Füßl M, Doccula FG, Navazio L, Fricker MD, Van Aken O, Finkemeier I, Meyer AJ, Szabò I, Costa A, Schwarzländer M (2015) The EF-hand Ca2+ binding protein MICU choreographs mitochondrial Ca2+ dynamics in Arabidopsis. The Plant Cell 27: 3190–3212
Pubmed: Author and Title
Google Scholar: Author Only Title Only Author and Title